The effects of oblique incidences on the XB mode conversion in the electron cyclotron range of frequency

Guozhang Jia, and Zhe Gao

Citation: Physics of Plasmas **24**, 022506 (2017); doi: 10.1063/1.4976324
View online: https://doi.org/10.1063/1.4976324
View Table of Contents: http://aip.scitation.org/toc/php/24/2
Published by the American Institute of Physics

The effects of oblique incidences on the XB mode conversion in the electron cyclotron range of frequency

Guozhang Jia[1,2] and Zhe Gao[3]
[1]*Institute of Plasma Physics, Chinese Academy of Sciences, Hefei 230031, China*
[2]*Center for Magnetic Fusion Theory, Chinese Academy of Sciences, Hefei 230031, China*
[3]*Department of Engineering Physics, Tsinghua University, Beijing 100084, China*

(Received 10 November 2016; accepted 30 January 2017; published online 15 February 2017)

The linear conversion from a fast extraordinary mode to a Bernstein mode (XB) in the electron cyclotron range of frequency is revisited numerically by using a simplified kinetic model. The corresponding wave equations are solved as a standard two-point boundary value problem, where the self-consistent boundary conditions are applied and the scattering coefficients are calculated accordingly. The numerical calculation of the XB conversion efficiency is compared with the analytical formula for the normal incidence (along the direction perpendicular to the equilibrium magnetic field and parallel to the density gradient), where a reasonable agreement is found. The effects of incident angles represented by refractive indexes on the conversion efficiency are analyzed. It is shown that as the incident angle deviates from the normal incidence, the efficiency of XB conversion decreases significantly. The results also indicate that the power loss in the XB process can be ascribed to the reflected fast extraordinary mode and the reflected-converted ordinary mode. The symmetry of the conversion efficiency about the incident angle is discussed, and the rigid restriction on the scale length of the density variation for effective XB conversions can be possibly alleviated through altering the injection direction in realistic experiments. *Published by AIP Publishing.*
[http://dx.doi.org/10.1063/1.4976324]

I. INTRODUCTION

Radio-frequency waves in the electron gyro-frequency range have distinct advantages for plasma heating and current drive in Tokamaks. Chief among these advantages include a launcher far away from the plasma, efficient coupling to the plasma at the edge, and high localization of the power deposition.[1] Meanwhile, fusion product benefits from high-β plasmas which are characterized by the relatively low magnetic field and high density (the electron plasma frequency $\omega_{pe} = \sqrt{n_e e^2/(\varepsilon_0 m_e)}$ is much larger than the electron cyclotron frequency $\omega_{ce} = eB_0/m_e$), but this meets with the accessibility limit of the electromagnetic ordinary mode (O-mode) and extraordinary mode (X-mode), and thus constrains the applications of the usual electron cyclotron resonance heating and current drive techniques. Electron Bernstein waves (EBWs), which exist in hot magnetized plasmas as quasi-electrostatic modes, can freely propagate in over-dense plasmas and can be efficiently absorbed by electrons in a wide range of cyclotron harmonics. Therefore, applications of EBWs in fusion plasma physics have been paid considerable attention in the past years[2] (and references therein).

EBWs can only be excited inside the plasmas due to its quasi-electrostatic nature. The XB mode conversion process is an effective approach to excite the EBW.[3–5] In this scheme, a fast X-mode launched from the vacuum into the plasma with a very steep density gradient tunnels through the evanescent layer between the right-cutoff and the left-cutoff, and then couples to the slow X-mode which in turn converts to the EBW in the vicinity of the upper hybrid resonance (UHR, a cold-plasma resonance), as illustrated in Fig. 1. The right-cutoff, left-cutoff, and the UHR in-between form a structure of the resonator.[6] An analytical expression of the XB conversion efficiency was derived for the normal incidence where the refractive indexes in the homogeneous y and z directions are zero, $N_y = N_z = 0$.[3] Recently, Kim *et al.*[7] investigated the effects of oblique injections (i.e., finite N_y and N_z, representing different incident angles) on the XB process by using a 1D full wave cold plasma model in which an artificial collisional absorption is necessary in order to eliminate the singularity of the UHR, and the conversion efficiency is represented by the collisional absorption rate.

In this paper, we solved the wave equations of the simplified kinetic model where the singularity is resolved and the EBW is naturally included. As a result, the XB conversion coefficient can be directly calculated. The numerical conversion efficiency is compared with the analytical formula under the normal incidence ($N_y = 0$, $N_z = 0$). The self-consistent waveform throughout the entire conversion region containing the information of the Bernstein mode can be acquired, and can be directly used to benchmark some nonlinear codes (for example, particle-in-cell) in linear regime. Then, we investigate the effects of finite N_y and N_z on the XB mode conversion. Based on our calculations, we find that the conversion efficiency is symmetric on N_z, but is asymmetric on N_y. The polarizations of X mode (and thus the phase difference between the X-mode propagating toward the L-cutoff and the reflected component propagating toward the UHR) can be varied by the sign of N_y. The method to alleviate the constriction on a scale length of plasma density variation is proposed for the first time, to our knowledge, by

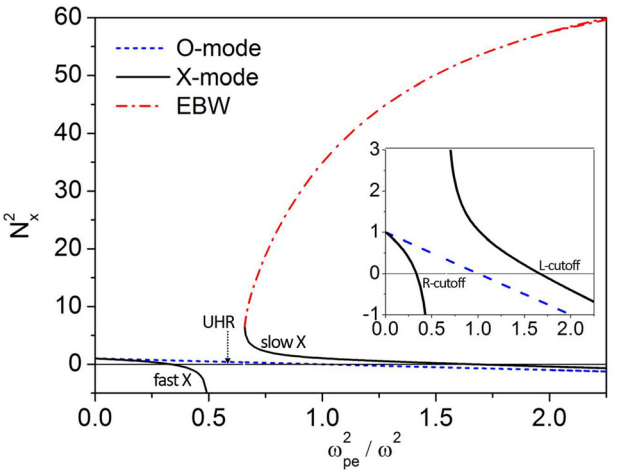

FIG. 1. Dispersion curves (the squared refractive index in the x direction as a function of the normalized electron density) for the simplified kinetic model, where the O-mode (dash blue), X-mode (solid black), and the Bernstein mode (dashed-dotted red) are included.

using a proper $N_y < 0$. This provides a possible approach to improve the conversion efficiency for electron Bernstein wave heating experiments, especially for those limited by density scale length. In our study, we use a slab geometry since this process occurs within a thin region, and assume that the equilibrium magnetic field is constant and in the z direction. The density varies only in the x direction.

The rest of this paper is organized as follows. In Sec. II, we demonstrate the wave equations modeling the X-B conversion. Comparison between the numerical results and the analytical formula under perpendicular incidence ($N_y = 0$, $N_z = 0$), and the effects of finite N_y and N_z on the conversion efficiency are given in Sec. III. In Sec. IV, summary and discussions are presented.

II. EQUATIONS AND BOUNDARY CONDITIONS OF 1D FULL WAVE KINETIC MODEL

Since the plasma system considered in this work is uniform both in y and z directions, the dependences of the wave fields on y, z, and t can be written as $\exp(-i\omega t + ik_y y + ik_z z)$, where k_y and k_z denote wave numbers in y and z directions, respectively. The Bernstein mode can be introduced by expanding the K_1 component of the kinetic dielectric tensor[8] to the 1st order in v_{Te}^2, $K_1 = K_{1c} - 3\omega_{pe}^2 k_\perp^2 v_{Te}^2/(\omega^2 - \omega_{ce}^2)/(\omega^2 - 4\omega_{ce}^2)$ where v_{Te} is the electron thermal velocity and K_{1c} is the zero-temperature limit of K_1, while other dielectric tensor elements are in the cold plasma limit. Making inverse Fourier transformation[8] $k_x \sim -id/dx$, the combined Maxwell-Vlasov system can be written as[3]

$$\frac{d\vec{F}_K}{d\xi} = i\vec{A}_K \cdot \vec{F}_K, \tag{1}$$

where $\vec{F}_K^{\mathrm{T}} = (E_{1x}, E_{1y}, E_{1z}, i\tilde{\chi}E'_{1x}, cB_{1z} - cB_{1y})$ is the field vector, $\xi \equiv x\omega/c$,

$$\tilde{\chi} = \frac{-3\omega^2\omega_{pe}^2 v_{te}^2/c^2}{(\omega^2 - \omega_{ce}^2)(\omega^2 - 4\omega_{ce}^2)},$$

and

$$\vec{A}_K = \begin{bmatrix} 0 & 0 & 0 & -\tilde{\chi}^{-1} & 0 & 0 \\ N_y & 0 & 0 & 0 & 1 & 0 \\ N_z & 0 & 0 & 0 & 0 & 1 \\ K_{1c} & K_{2c} & 0 & 0 & N_y & N_z \\ -K_{2c} & K_{1c} - N_z^2 & N_y N_z & 0 & 0 & 0 \\ 0 & N_y N_z & K_{3c} - N_y^2 & 0 & 0 & 0 \end{bmatrix},$$

with $N_y = k_y c/\omega$ and $N_z = k_z c/\omega$. K_{1c}, K_{2c}, and K_{3c} are the dielectric tensor elements in the cold plasma limit

$$K_{1c} = 1 - \frac{\omega_{pe}^2}{\omega^2 - \omega_{ce}^2},$$

$$K_{2c} = i\frac{\omega_{ce}\omega_{pe}^2}{\omega(\omega^2 - \omega_{ce}^2)},$$

$$K_{3c} = 1 - \frac{\omega_{pe}^2}{\omega^2}.$$

In this study, we concentrate mainly on the characteristics of the power partition among distinct modes involved in the XB process and neglect the effect of damping. Therefore, we select $B_0 = 0.12\,\mathrm{T}$ and $f = 5\,\mathrm{GHz}$ ($\omega = 1.5\omega_{ce}$) in order to avoid damping. The density profile is expressed as $n_e = n_O + 0.9n_O \tanh[(\xi - 0.5a)/\xi_w]$, where $n_O = 3.1 \times 10^{17}\,\mathrm{m}^{-3}$ is the density corresponding to $\omega^2 = \omega_{pe}^2$ at $\xi = 0.5a$, $a = \omega/c$ is the normalized total length of the calculation, and ξ_w is related to the scale length of density variation through the definition at $\xi = 0.5a$

$$\frac{1}{L_n} = \frac{\omega}{c}\frac{dn_e}{n_e d\xi}\bigg|_{\xi=0.5a}.$$

The resulted density distributions near the calculation boundaries $x_1 = 0$ and $x_2 = a$ are flat, and the x components of the wave-numbers and the polarizations for different modes can be well separated so that the scattering coefficients can be well defined. The boundary conditions in the XB process are chosen as follows to include all the possible modes.[9,10] There might be a reflected fast X mode, an exponentially decaying mode, and a reflected-converted O mode at the low-density side of the conversion layer for a fast X mode incident at $x_1 = 0$. Meanwhile, at the high-density boundary ($x_2 = a$), a transmitted slow X mode, a tunneled-converted O mode, and a converted Bernstein mode might exist. Of course, it will be noted that not all the modes should exist at the same time, and the realistic status depends on the calculation results. The amplitude of particular polarization component (E_x in our calculation) can be assumed for every possible mode, and the related Poynting vector can be also represented. These to-be-solved amplitudes are superposed to give the total field (total E_x) and an algebraic equation is obtained. Algebraic equations for other polarization components (E_y, E_z, etc.) can be obtained in a similar manner. The boundary conditions can be determined by the requirement of nontrivial solutions.[9] The set of 1st order ordinary equations (1) can be solved as a standard two-point boundary value problem by using a finite difference solver in

MATLAB, which implements the 3-stage Lobatto IIIa formula. The largest relative error of the wave field is 10^{-6}.

Using the numerical results, the x-component of Poynting vectors (P_x) for every mode can be acquired. Therefore, the conversion, reflection, and transmission coefficients can be defined directly through the ratios between P_x of the different modes to that of the incident fast X wave.

III. RESULTS AND DISCUSSION

A. Comparison with analytical formula for normal incidence

First, we compare the numerical XB conversion efficiency under the normal incidence ($N_y = N_z = 0$) with the analytical formula for a uniform magnetic field, which is rewritten as[3]

$$C_{XB} = 4e^{-\pi\eta}(1 - e^{-\pi\eta})\cos^2(\varphi/2 + \theta) \equiv C_{\max}\cos^2(\phi/2 + \theta), \quad (2)$$

η is the Budden parameters,

$$\eta \simeq \frac{\omega_{ce}^2 L_n}{c\omega_{pe}}\left(\sqrt{1 + \omega_{pe}^2/\omega_{ce}^2} - 1\right)^{1/2}\Big|_{UHR}, \quad (3)$$

ϕ is the phase difference between the slow X-mode propagating toward the L-cutoff and the reflected component propagating toward the UHR, and θ is the phase of the Gamma function $\Gamma(-i\eta/2)$. The density difference between L-cutoff and UHR is 5 times larger than the density difference between the UHR and R-cutoff under our parameters. Thus, we applied the formula (17) in Ref. 6 for ϕ which is approximately reduced as $\phi = 3.9L_n\omega_{ce}/c + \pi/2$. The comparison between the numerical result and the formula is given in Fig. 2, where a reasonable agreement is shown. The optimal scale length of density variation predicted by the formula is 5.07 mm and the numerical value is 4.69 mm. The discrepancy may be due to the phases ϕ and θ in Eq. (2) which was derived based on the local expansion of the density profile in

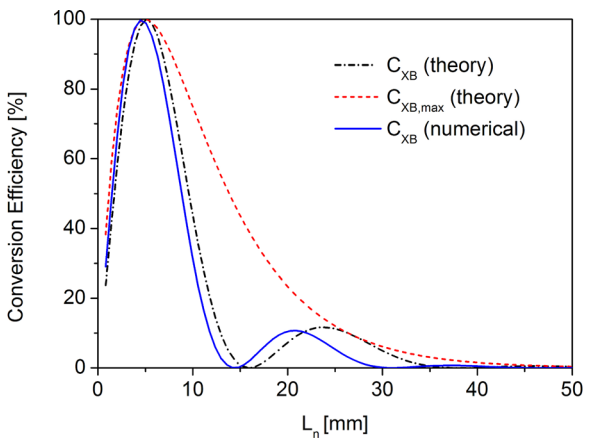

FIG. 2. Comparison of the XB conversion efficiency between the numerical calculation (solid blue) and the analytic formula (dashed-dotted black) for $N_y = 0$ and $N_z = 0$, where $B_0 = 0.12$ T and $f = 5$ GHz. The maximum conversion efficiency (short dash red) is the envelope of the analytic formula.

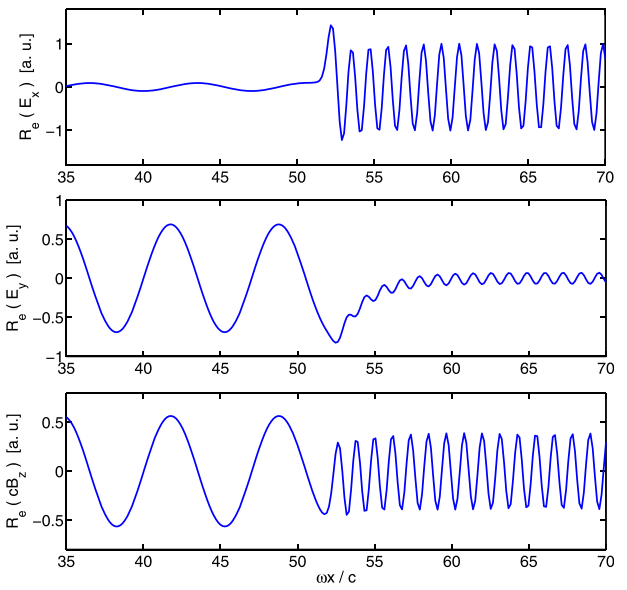

FIG. 3. Wave patterns for the complete conversion from a fast X mode to a Bernstein mode, where $N_y = 0$, $N_z = 0$, and $L_n = 4.69$ mm.

Ref. 6. However, both 5.07 mm and 4.69 mm are rigorous conditions for realistic experiments.

The wave patterns for $L_n = 4.69$ mm are demonstrated in Fig. 3. It is shown that a y-polarized fast X-mode at the low-density side of the UHR transforms into an x-polarized Bernstein mode at the high-density side. The wave patterns for $L_n = 14.2$ mm, where the XB conversion efficiency is 0, are demonstrated in Fig. 4. The incident y-polarized fast X-mode is totally reflected ($R_X = 100\%$) at the evanescent layer forming a standing wave, and there is no x-polarized Bernstein mode excited at the high-density side.

B. Effects of oblique incidences

The effects of oblique injections (finite N_y and N_z) on the conversion efficiency cannot be predicted by the analytic formula, Eq. (2), which was derived based on the assumption

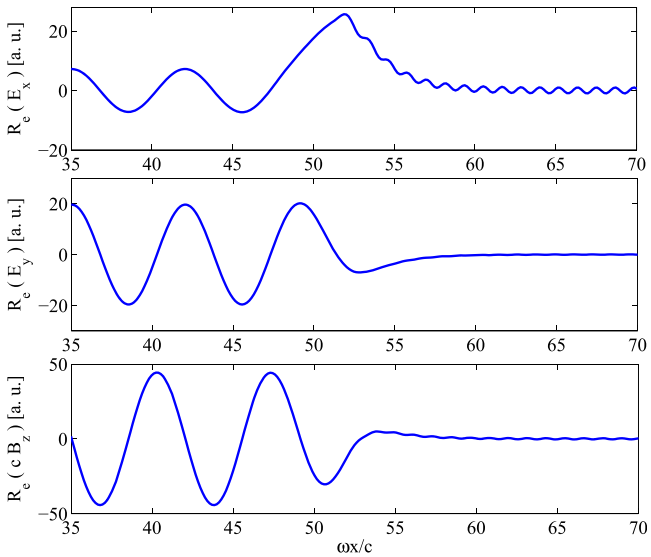

FIG. 4. Wave patterns for $C_{XB} = 0$ and $R_X = 100\%$, where $N_y = N_z = 0$ and $L_n = 14.2$ mm.

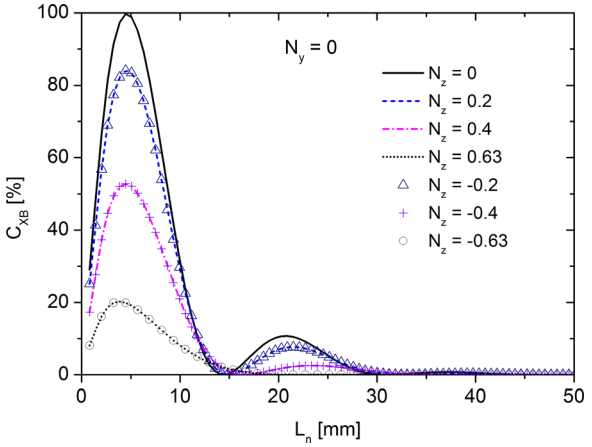

FIG. 5. Dependences of C_{XB} on the scale length of density variation for $N_z = 0$ (solid black), 0.2 (short-dash blue), 0.4 (dashed-dotted pink), 0.63 (dot black), −0.2 (triangle), −0.4 (cross), and −0.63 (circle) where $N_y = 0$.

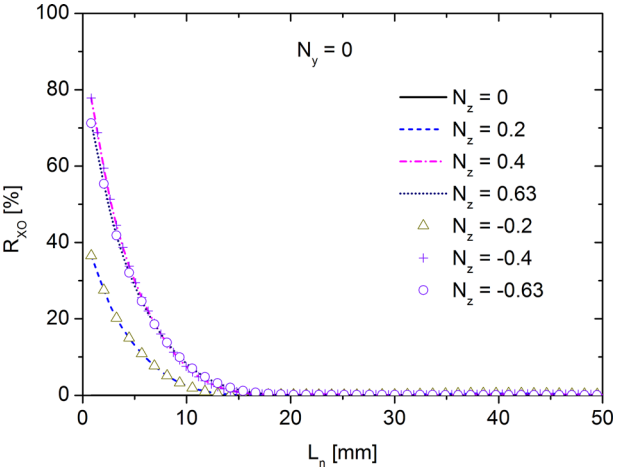

FIG. 7. Dependences of R_{XO} on the scale length of density variation for $N_z = 0$ (solid black), 0.2 (short-dash blue), 0.4 (dashed-dotted pink), 0.63 (dot black), −0.2 (triangle), −0.4 (cross), and −0.63 (circle) where $N_y = 0$.

of $N_y = N_z = 0$. The numerical results for non-zero N_y and N_z are shown in Figs. 5–9.

For $N_y = 0$, the XB conversion efficiency decreases as N_z increases, as shown in Fig. 5. The slow X-mode can be mode-converted to O-mode by the reverse process of the OX mode conversion[11] due to the short density scale length and the finite N_z. The decrease of conversion efficiency is ascribed to the reflected fast X-mode (R_X) and the reflected-converted O-mode (R_{XO}) as depicted in Figs. 6–7. Meanwhile, the optimal density scale length shows little dependences on N_z except for very large N_z (≥ 0.63). Meanwhile, by making some derivatives and algebraic recombinations, the modeling equations (1) can be transformed into the following two differential equations for $N_y = 0$ to see its symmetry:

$$d^2E_y/d\xi^2 - K_2E_x + \left(K_1 - N_z^2\right)E_y = 0, \tag{4}$$

$$\frac{d^4\left(i\tilde{\chi}E_x'\right)}{d\xi^4} + \left(K_3 - \frac{K_1}{\tilde{\chi}}\right)\frac{d^2\left(i\tilde{\chi}E_x'\right)}{d\xi^2} - \left(K_1 - N_z^2\right)\frac{K_3}{\tilde{\chi}}\left(i\tilde{\chi}E_x'\right) - iK_2\frac{d^3E_y}{d\xi^3} - iK_2K_3\frac{dE_y}{d\xi} = 0, \tag{5}$$

which depend only on N_z^2. Therefore, C_{XB} is symmetric about N_z and does not depend on its sign.

For $N_z = 0$, the overall XB conversion efficiency decreases also as N_y increases, as shown in Fig. 8. C_{XB}–L_n curve shows a strong dependence on N_y and is also asymmetric about N_y. Mathematically, the asymmetry on N_y is intrinsic since the wave equations contain odd order terms of N_y. Physically, the sign of N_y varies the polarizations of X mode, and therefore, the phase difference between slow X-mode propagating toward the L-cutoff and the reflected component propagating toward the UHR can be altered by N_y. We can choose a negative N_y to shift the peak of C_{XB} (and the window of effective conversion) to a larger L_n and thus to alleviate the rigid restriction on the density profile at the cost of dropping a certain conversion efficiency. The decrease of $C_{XB,\max}$ is ascribed to the reflected X-mode as shown in Fig. 9, while the reflected-converted O-mode is negligible due to the decoupling of O-mode from the X-mode and EBW.

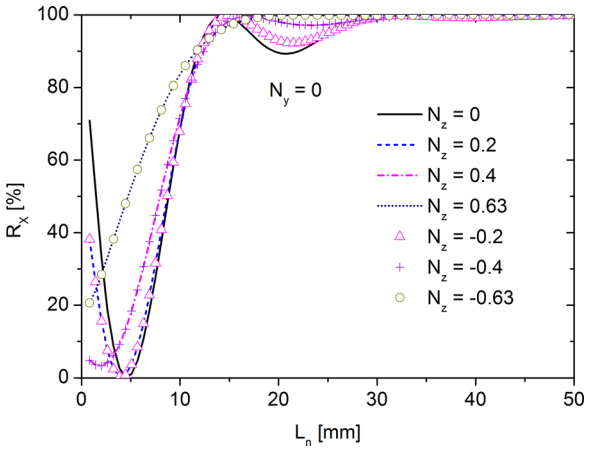

FIG. 6. Dependences of R_X on the scale length of density variation for $N_z = 0$ (solid black), 0.2 (short-dash blue), 0.4 (dashed-dotted pink), 0.63 (dot black), −0.2 (triangle), −0.4 (cross), and −0.63 (circle) where $N_y = 0$.

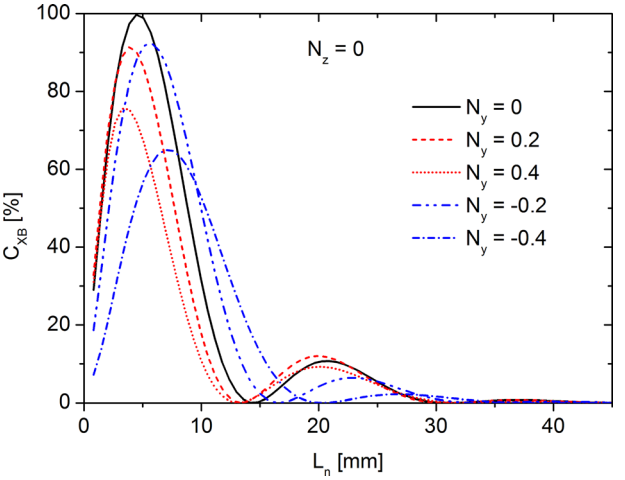

FIG. 8. Dependences of C_{XB} on the scale length of density variation for $N_y = 0$ (solid black), 0.2 (short-dash red), 0.4 (dot red), −0.2 (dashed-dotted-dotted blue), and −0.4 (dashed-dotted blue) where $N_z = 0$.

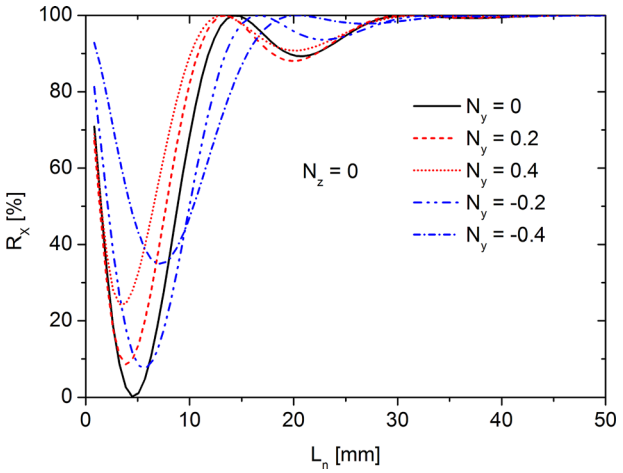

FIG. 9. Dependences of R_X on the scale length of density variation for $N_y = 0$ (solid black), 0.2 (short-dash red), 0.4 (dot red), −0.2 (dashed-dotted-dotted blue), and −0.4 (dashed-dotted blue) where $N_z = 0$.

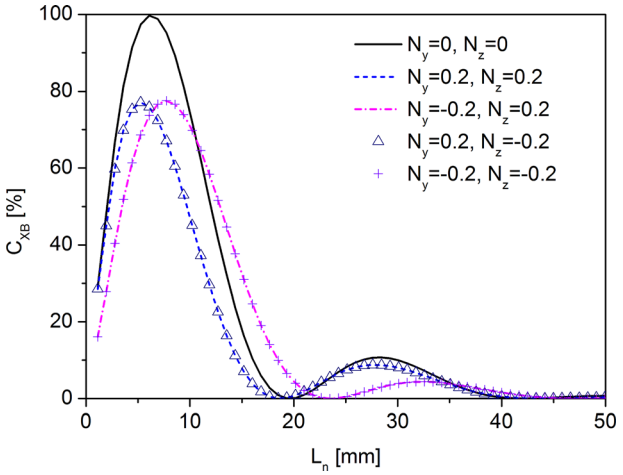

FIG. 10. Dependences of C_{XB} on the scale length of density variation for $(N_y, N_z) = (0,\ 0)$ (solid black), (0.2, 0.2) (short-dash blue), (−0.2 0.2) (dashed-dotted pink), (0.2, −0.2) (triangle), and (−0.2, −0.2) (cross).

Both N_y and N_z degenerate the efficiency of XB conversion, and their influences show the accumulative behavior, as illustrated in Fig. 10. Therefore, we should choose normal incidence when the optimal scale length of density variation is available, and otherwise, we can select a proper N_y to shift the window of effective XB conversion while maintaining $N_z = 0$.

IV. SUMMARY

The XB mode conversion is analyzed by using the simplified kinetic model in which the kinetic mode (EBW) is naturally included and the singularity of cold resonance is eliminated. The effects of oblique propagations are included. Conversion efficiency shows agreement with the theoretical formula for $N_y = N_z = 0$. C_{XB} is decreased by the effects of the oblique propagation (finite N_y or N_z). The scale length corresponding to the peak of C_{XB}–L_n curve, $L_{n,\max}$, shows less dependence on N_z except for very large values ($N_z \geq 0.63$), but N_y varies with $L_{n,\max}$ significantly. C_{XB} is symmetric about N_z, but asymmetric about N_y, although the sign of N_y or N_z does not influence the dispersion relation.

Effective XB conversion requires very steep density profile (the optimal scale length is small) so that the incident X mode can tunnel through the evanescent region. However, extreme small L_n may not be realized due to the limit of some instabilities, and the conversion efficiency decreases drastically as L_n deviates from the optimal value. Based on our calculations, we find that the window for effective XB conversion can be shifted towards larger L_n (the peak efficiency drops a bit, but can still be greater than 50%). We propose that the restriction on L_n in realistic XB experiments can be alleviated by varying the launching angles related to the negative N_y at the expense of losing certain conversion efficiency. For example, as shown in Figure 8, the optimal L_n is 4.69 mm ($N_y = N_z = 0$, $C_{XB} = 100\%$). If we can only decrease L_n to 10 mm, C_{XB} decreases to 50% for $N_y = N_z = 0$, but we can acquire $C_{XB} \approx 70\%$ for $N_z = 0$ and $N_y = -0.2$.

ACKNOWLEDGMENTS

This work was supported by the NSFC under Grant Nos. 11505227, 11475220, 11405218, 11405208, 11261140327, and 11325524, the program of Fusion Reactor Physics and Digital Tokamak with the CAS "One-Three-Five" Strategic Planning, the JSPS-NRF-NSFC A3 Foresight Program in the field of Plasma Physics (NSFC: No. 11261140328 and NRF: No. 2012K2A2A6000443), and the National Magnetic Confinement Fusion Science Program of China with Grant Nos. 2013GB111002, 2013GB112010, 2013GB112001, and 2015GB101003.

[1]R. Prater, "Heating and current drive by electron cyclotron waves," Phys. Plasmas **11**(5), 2349–2376 (2004).
[2]H. P. Laqua, "Electron Bernstein wave heating and diagnostic," Plasma Phys. Controlled Fusion **49**(4), R1–R42 (2007).
[3]A. K. Ram and S. D. Schultz, "Excitation, propagation, and damping of electron Bernstein waves in tokamaks," Phys. Plasmas **7**(10), 4084–4094 (2000).
[4]G. Taylor, P. C. Efthimion, B. Jones, B. P. LeBlanc, J. R. Wilson, J. B. Wilgen, G. L. Bell, T. S. Bigelow, R. Maingi, D. A. Rasmussen, R. W. Harvey, A. P. Smirnov, F. Paoletti, and S. A. Sabbagh, "Enhanced conversion of thermal electron Bernstein waves to the extraordinary electromagnetic mode on the National Spherical Torus Experiment," Phys. Plasmas **10**(5), 1395–1401 (2003).
[5]P. K. Chattopadhyay, J. K. Anderson, T. M. Biewer, D. Craig, C. B. Forest, R. W. Harvey, and A. P. Smirnov, "Electron Bernstein wave emission from an overdense reversed field pinch plasma," Phys. Plasmas **9**(3), 752–755 (2002).
[6]A. K. Ram, A. Bers, S. D. Schultz, and V. Fuchs, "Mode conversion of fast Alfven waves at the ion-ion hybrid resonance," Phys. Plasmas **3**(5), 1976–1982 (1996).
[7]S. H. Kim, H. Y. Lee, J. G. Jo, and Y. S. Hwang, "One-dimensional full wave simulation on XB mode conversion in electron cyclotron heating," Phys. Plasmas **21**(6), 062108 (2014).
[8]D. G. Swanson, *Theory of Mode Conversion and Tunneling in Inhomogeneous Plasmas* (Wiley, 1998).
[9]G. Z. Jia and Z. Gao, "One dimensional full wave analysis of slow-to-fast mode conversion in lower hybrid frequencies," Phys. Plasmas **21**(12), 122121 (2014).
[10]C. Y. Wang, M. D. Carter, D. B. Batchelor, and E. F. Jaeger, "Numerical solution of a tunneling equation," No. ORNL/TM–12721 (Oak Ridge National Lab., TN 1994), available at https://www.osti.gov/scitech/biblio/10167991.
[11]J. Preinhae and V. Kopecky, "Penetration of high-frequency waves into a weakly inhomogeneous magnetized plasma at oblique-incidence and their transformation to Bernstein modes," J. Plasma Phys. **10**, 1–12 (1973).